Impedance Scan of Inverter-Based Resources and Diesel Generator for Stability Analysis

Preprint

Soham Chakraborty, Jing Wang, Subhankar Ganguly, and Benjamin Kroposki

National Renewable Energy Laboratory

Presented at the 2024 IEEE Power and Energy Society General Meeting
Seattle, Washington
July 21–25, 2024

NREL is a national laboratory of the U.S. Department of Energy
Office of Energy Efficiency & Renewable Energy
Operated by the Alliance for Sustainable Energy, LLC

This report is available at no cost from the National Renewable Energy Laboratory (NREL) at www.nrel.gov/publications.

Contract No. DE-AC36-08GO28308

Conference Paper
NREL/CP-5D00-88130
August 2024

Impedance Scan of Inverter-Based Resources and Diesel Generator for Stability Analysis

Preprint

Soham Chakraborty, Jing Wang, Subhankar Ganguly, and Benjamin Kroposki

National Renewable Energy Laboratory

Suggested Citation
Chakraborty, Soham, Jing Wang, Subhankar Ganguly, and Benjamin Kroposki. 2024. *Impedance Scan of Inverter-Based Resources and Diesel Generator for Stability Analysis: Preprint*. Golden, CO: National Renewable Energy Laboratory. NREL/CP-5D00-88130. https://www.nrel.gov/docs/fy24osti/88130.pdf.

NREL is a national laboratory of the U.S. Department of Energy
Office of Energy Efficiency & Renewable Energy
Operated by the Alliance for Sustainable Energy, LLC

This report is available at no cost from the National Renewable Energy Laboratory (NREL) at www.nrel.gov/publications.

Contract No. DE-AC36-08GO28308

Conference Paper
NREL/CP-5D00-88130
August 2024

National Renewable Energy Laboratory
15013 Denver West Parkway
Golden, CO 80401
303-275-3000 • www.nrel.gov

NOTICE

This work was authored by the National Renewable Energy Laboratory, operated by Alliance for Sustainable Energy, LLC, for the U.S. Department of Energy (DOE) under Contract No. DE-AC36-08GO28308. Funding provided by Funding provided by the U.S Department of Energy Office of Energy Efficiency and Renewable Energy Solar Energy Technologies Office Agreement Number 38637. The views expressed herein do not necessarily represent the views of the DOE or the U.S. Government. The U.S. Government retains and the publisher, by accepting the article for publication, acknowledges that the U.S. Government retains a nonexclusive, paid-up, irrevocable, worldwide license to publish or reproduce the published form of this work, or allow others to do so, for U.S. Government purposes.

Cover Photos by Dennis Schroeder: (clockwise, left to right) NREL 51934, NREL 45897, NREL 42160, NREL 45891, NREL 48097, NREL 46526.

Impedance Scan of Inverter-Based Resources and Diesel Generator for Stability Analysis

Soham Chakraborty, Jing Wang, Subhankar Ganguly, Benjamin Kroposki
Power Systems Engineering Center, National Renewable Energy Laboratory, Golden, Colorado 80401, USA.
{soham.chakraborty, jing.wang, subhankar.ganguly, benjamin.kroposki}@nrel.gov

***Abstract*—Impedance-based methods are widely used for power system stability analysis with inverter-based resources (IBRs), e.g., assessing dynamic interactions between the power grid and an IBR, control interactions between multiple IBRs, and the sub-synchronous oscillation and damping phenomenon. Since it is difficult to get a numerical model 100% matching with the hardware IBR, using the hardware inverter directly to obtain its output impedance has become a prominent approach nowadays. Therefore, this article presents the impedance scan using hardware IBRs, and also a hardware diesel generator as it still stays with the grid before the grid completely goes to renewable. The devices under test (DuTs) for the impedance scan includes two 3-ϕ, 480 V, 60 Hz commercial grid-forming IBRs (one of 250 kVA and another of 125 kVA rating) in series with Δ-Y transformers, one 3-ϕ, 480 V, 60 Hz commercial grid-following IBR (of 125 kVA rating), and a 3-ϕ, 480 V, 60 Hz commercial diesel generator (of 187.5 kVA rating). Using voltage signals perturbed with sub-, inter-, and higher harmonic components, and measuring the current response, the positive-sequence impedances are computed via an offline-based post-analysis. Moreover, best-fit transfer functions are estimated that closely resemble the measured data points of the positive-sequence impedances. Based on the observations from various outcomes of the hardware experiments, this article also provides some fundamental insights on the equivalent positive-sequence impedance of a combination of multiple hardware components by comparing the estimated and the empirically computed impedances. A comparative insight on the damping capability of the DuTs using the positive-sequence impedances of the hardware is also discussed.**

I. Introduction

As increasingly more inverter-based resources (IBRs) are integrated into power systems, the dynamic stability of power grids needs to be investigated as the grid becomes weaker and has less inertia [1]; therefore, the study of system strength and the stability of IBR-dominant grids is an active topic today. For example, subsynchronous oscillations have been observed in real-world photovoltaic power plants, and analytical verification and electromagnetic transient (EMT) studies are performed to identify the sources of oscillations and instabilities, including communication delays between the plant controller and the inverter, high volt/var sensitivity at higher power levels, and inverter control and grid impacts [2]. Small-signal analysis-based stability studies are widely performed for systems with grid-forming (GFM) and grid-following (GFL) IBRs, and eigenvalues are computed to investigate the stability of power systems with varying control parameters and operation modes for IBRs [3]. The large-signal nonlinear state-space model for IBR-dominant microgrids is developed in [4], and Lyapunov-based stability sensitivity analyses are performed under three dynamic events to identify the solutions for stability improvement, e.g., inverter droop control. The geometric method is similar to the Lyapunov-based approach; it uses the joints of the stable manifolds of the unstable points to determine the stability region of a system [5]. This is an evolving research area, and increasingly advanced stability analytical methods, tools, and frameworks (e.g., stability indices and system strengths) are being researched and developed to improve the robustness and scalability of the developed approaches. Reference [1] gives an overview of the state of the art in stability analysis in IBR-dominant systems; the summarized techniques are presented in Fig. 1.

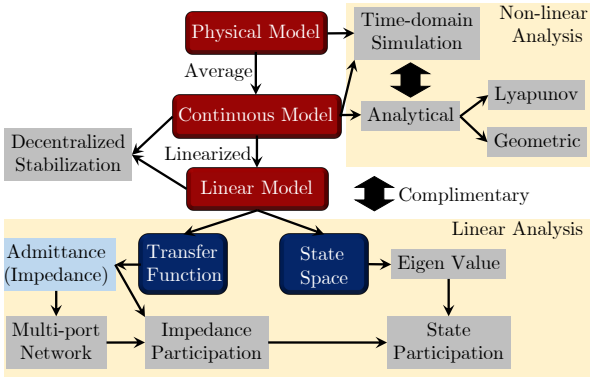

Fig. 1: Overview of the state-of-the-art power system stability analysis for IBR-dominant systems [1].

Among all the approaches, the positive-/negative-sequence impedance-based approach has been widely used in academia and industry as an effective stability analysis tool for IBR-dominant systems. Reference [6] comprehensively illustrates the common impedance-based approaches, including impedances in the d-q domain, the sequence domain, and the phasor domain. Validation examples through EMT and controller-hardware-in-the-loop-based simulations are given for each method to show their pros and cons. Further, impedance-based approaches provide insight into an IBR's damping capability when the IBR can be formulated as a

This work was authored by the National Renewable Energy Laboratory, operated by Alliance for Sustainable Energy, LLC, for the U.S. Department of Energy (DOE) under Contract No. DE-AC36-08GO28308. Funding provided by the U.S Department of Energy Office of Energy Efficiency and Renewable Energy Solar Energy Technologies Office Agreement Number 38637. The views expressed in the article do not necessarily represent the views of the DOE or the U.S. Government. The U.S. Government retains and the publisher, by accepting the article for publication, acknowledges that the U.S. Government retains a nonexclusive, paid-up, irrevocable, worldwide license to publish or reproduce the published form of this work, or allow others to do so, for U.S. Government purposes.

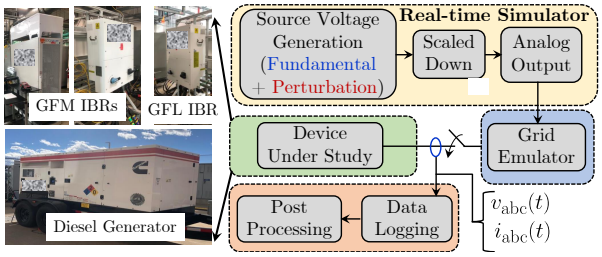

Fig. 2: Laboratory-based experimental setup with ScopeCorder for data logging with sampling rate of 50K samples/s and 16-bit analog resolution and 300 kHz bandwidth analog voltage sensor.

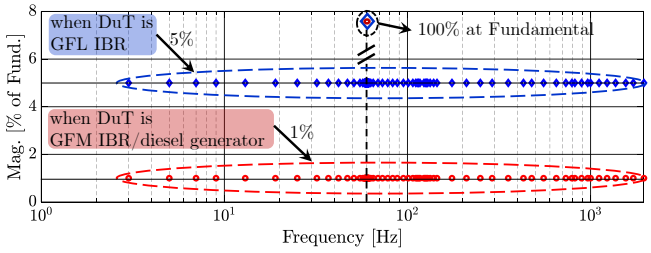

Fig. 3: Magnitude of the injected positive-sequence voltage perturbation at various frequencies injected for the impedance scan tests.

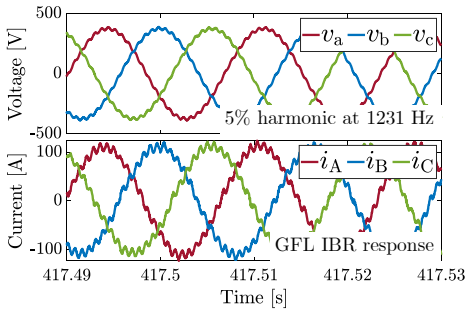

Fig. 4: A sample voltage waveform perturbed with $f_h = 1231$ Hz of 5% of the fundamental waveform and the corresponding steady-state output current response of the GFL IBR-based DuT.

second-order system based on the transfer function [7]. This shows promising applications and requires more research work as increasingly more grid codes and/or interconnection agreements require GFL/GFM IBRs to provide active damping capability. Moreover, the entire class of passivity-based stability analysis, as referred in [8], uses the equivalent impedance model of IBRs connected to the grid in series with a equivalent grid impedance. The main contributions of this article are summarized as follows:

- This article measures the positive-sequence impedance of a hardware device in a large-scale laboratory environment. Various types of hardware components are characterized, including GFL IBRs, GFM IBRs, and diesel generators. Documenting the nature and characteristics of the positive-sequence impedances of these power system components will provide the platform for further analyzing the impedance/admittance-based passivity analysis for assessing the system stability with such components under operation.
- This article provides some fundamental insights based on observations from various outcomes of the hardware experiments, including the equivalent positive-sequence impedance of a combination of multiple hardware components (GFM IBRs, GFL IBRs, diesel generators), empirical computations of positive-sequence impedances of such combinations, etc.
- This article provides insights on the damping capability of various active components (GFM IBRs, GFL IBRs, and diesel generators) using the positive-sequence impedance scan approach on the hardware testing data.

II. Computation of Positive-Sequence Impedance of Device Under Test

A. Hardware Setup Under Study

Fig. 2 shows the overall laboratory-based experimental setup that is used for scanning the frequency response of the DuTs: two 3-ϕ, 480 V, 60 Hz commercial GFM IBRs (one of 250 kVA and another of 125 kVA rating), one 3-ϕ, 480 V, 60 Hz commercial GFL IBR (of 125 kVA rating), and a 3-ϕ, 480 V, 60 Hz commercial diesel generator (of 187.5 kVA rating). A 4-quadrant controllable voltage source-based grid simulator with sufficient power capacity and operating in sinking mode is used to generate the perturbed voltage waveform across DuTs.

B. Testing Approach for Impedance Scan

It is common practice to apply a perturbed voltage signal across the DuT and measure both the terminal voltage, v_{abc}, and the resulting output current, i_{abc}, of the DuT to estimate the output impedance. As shown in Fig. 2, a real-time simulator is used to generate the perturbed voltage signal using the internal control blocks. Then, the perturbed signal can be brought out and sent to a power amplifier (grid emulator of Fig. 2), across which the DuT is connected. For each test, the perturbed voltage waveform contains: 1) the fundamental signal at the rated voltage (480 V line-to-line) and frequency (60 Hz) and 2) the harmonic signal of the magnitude of h% of the rated voltage (480 V line-to-line) at f_h Hz. For GFL IBRs, the magnitude of the harmonic component is selected as 5% (h = 5) and 1% (h = 1) of the fundamental waveform for the GFL IBR-based DuT and the GFM IBR/diesel generator-based DuT, respectively. It is important to mention here that the safe amount of perturbation is required to be judiciously selected based on the nature of the DuT (controlled current and voltage source for GFL and GFM units). It observe that when the DuT is GFL unit and GFM unit, the amount of perturbation can be selected up to 5% and 1% of the rated voltage without harming or causing IBR tripping, respectively. As shown in Fig. 3, the harmonic spectrum covers all subharmonic, interharmonic, and higher harmonic components from $f_h = 3$ Hz to $f_h = 1957$ Hz. For instance, Fig. 4 shows a sample voltage waveform perturbed with $f_h = 1231$ Hz of 5% of the fundamental waveform and the corresponding output current response (in steady state) of the GFL IBR-based DuT. During each test, the DuTs are always operated at 50% of the rating. All DuTs are individually tested as well as all together.

C. Calculation of Positive-Sequence Impedance Model

The instantaneous terminal-phase voltages of the DuT are denoted as $v_a(t)$, $v_b(t)$, and $v_c(t)$; and the instantaneous phase

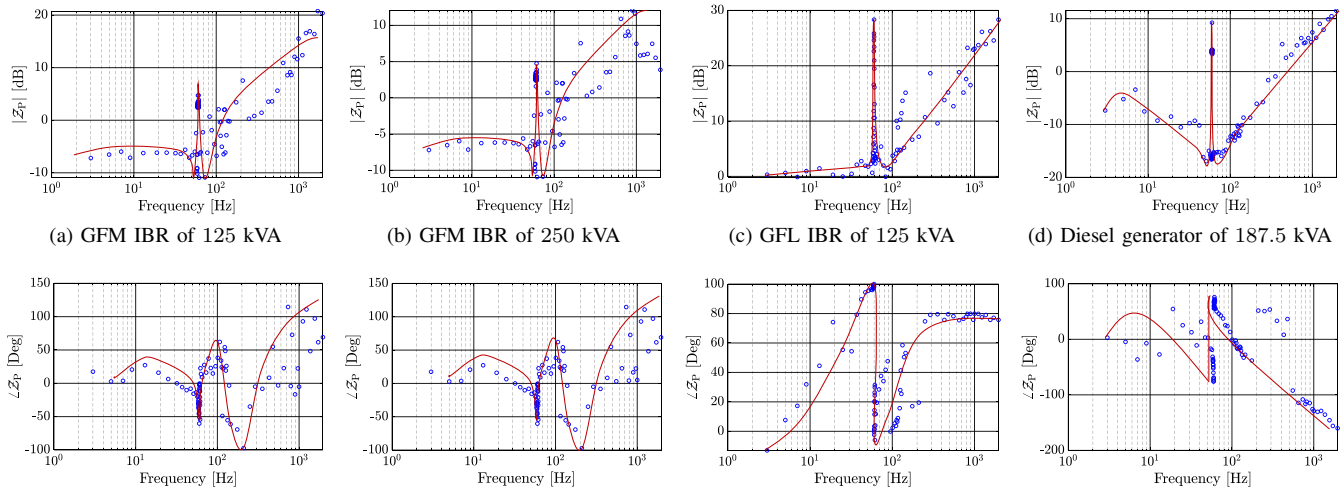

(a) GFM IBR of 125 kVA (b) GFM IBR of 250 kVA (c) GFL IBR of 125 kVA (d) Diesel generator of 187.5 kVA

(e) GFM IBR of 125 kVA (f) GFM IBR of 250 kVA (g) GFL IBR of 125 kVA (h) Diesel generator of 187.5 kVA

Fig. 5: The measured positive-sequence impedances of the DuTs measured individually.

currents are denoted as $i_{\rm a}(t)$, $i_{\rm b}(t)$, and $i_{\rm c}(t)$. The DuT was initially operating in steady state at its nominal fundamental frequency, $f_{\rm R}$ (Hz), and it is disturbed from its steady-state operation by injecting a small-signal perturbation in $v_{\rm a}(t)$, $v_{\rm b}(t)$, and $v_{\rm c}(t)$ at the positive-sequence frequency, $f_{\rm P}$. For linear analysis for a balanced steady-state operation of the DuT, the phase voltages of the DuT output in the time domain can be written as [9]–[12]:

$$v_{\rm a}(t) = V_{\rm R}\cos(\omega_{\rm R}t + \phi_{\rm v}^{\rm R}) + V_{\rm P}\cos(\omega_{\rm P}t + \phi_{\rm v}^{\rm P}),$$
$$v_{\rm b}(t) = V_{\rm R}\cos(\omega_{\rm R}t - \frac{2\pi}{3} + \phi_{\rm v}^{\rm R}) + V_{\rm P}\cos(\omega_{\rm P}t - \frac{2\pi}{3} + \phi_{\rm v}^{\rm P}),$$
$$v_{\rm c}(t) = V_{\rm R}\cos(\omega_{\rm R}t + \frac{2\pi}{3} + \phi_{\rm v}^{\rm R}) + V_{\rm P}\cos(\omega_{\rm P}t + \frac{2\pi}{3} + \phi_{\rm v}^{\rm P}),$$

where $V_{\rm R}$ and $V_{\rm P}$ are the amplitude of the voltage at the fundamental frequency, $\omega_{\rm R} := 2\pi f_{\rm R}$, and at the positive-sequence perturbed frequency, $\omega_{\rm P} := 2\pi f_{\rm P}$; and $\phi_{\rm v}^{\rm N}$ and $\phi_{\rm v}^{\rm P}$ are the initial phases of the fundamental and the positive-sequence perturbed signal. In other words, the phase voltage (for instant phase-a) in the frequency domain, $\bar{V}_{\rm a}(s)$, can be written as $\bar{V}_{\rm a}(s) = (V_{\rm R}/2)e^{j\phi_{\rm v}^{\rm R}}$ for $s = j\omega_{\rm R}$ and $\bar{V}_{\rm a}(s) = (V_{\rm P}/2)e^{j\phi_{\rm v}^{\rm P}}$ for $s = j\omega_{\rm P}$. As a result, the positive-sequence perturbation component of the voltage $\bar{V}_{\rm P} := \bar{V}_{\rm a}(j\omega_{\rm P})$. The resulting $i_{\rm a}(t)$, $i_{\rm b}(t)$, and $i_{\rm c}(t)$ can be similarly described. With this representation, the small-signal equivalent positive-sequence impedance of the DuT can be formulated as $\mathcal{Z}_{\rm P}(s) := \bar{V}_{\rm P}/\bar{I}_{\rm P}$.

III. Laboratory-Based Testing Results

A. Results for Individual DuTs Tested Separately

Based on the theoretical underpinnings discussed in Section II-C and the followed approach, the positive-sequence impedance of the DuTs at different perturbation frequencies are individually measured, as shown in Fig. 5. The measured magnitude of the positive-sequence impedance, $|\mathcal{Z}_{\rm P}|$ (in dB), of the GFM IBR of 125 kVA, the GFM IBR of 250 kVA, the GFL IBR of 125 kVA, and the diesel generator of 187.5 kVA are shown in Fig. 5(a), Fig. 5(b), Fig. 5(c), and Fig. 5(d), respectively. Similarly, the measured phase of the positive-sequence impedance, $\angle\mathcal{Z}_{\rm P}$ (in deg), of the GFM IBR of 125 kVA, the GFM IBR of 250 kVA, the GFL IBR of 125 kVA, and the diesel generator of 187.5 kVA are shown in Fig. 5(e), Fig. 5(f), Fig. 5(g), and Fig. 5(h), respectively. In all these figures, the blue circled data are the values computed based on the DuT measurements. Based on the measured data of the magnitude, $|\mathcal{Z}_{\rm P}|$, and phase, $\angle\mathcal{Z}_{\rm P}$, of the positive-sequence impedances of the different DuTs, the best-fit transfer functions are estimated using the '*tfest*' command of the 'System Identification Toolbox' of MATLAB. In the same figure, the Bode plots of the estimated transfer functions (piece-wise) are also shown in red. It is observed that the nature of the positive-sequence impedance transfer function, $\mathcal{Z}_{\rm P}(s)$, for the GFM IBR of rating 125 kVA is quite similar to that of the GFM IBR of rating 250 kVA. This observation demonstrates that the control functionality for GFM inverters (i.e., droop law-based control, outer-voltage inner-current control) along with the filter parameters for a generic GFM IBR ensure a particular nature of the $\mathcal{Z}_{\rm P}(s)$, which is independent of the rating of the IBR. It is also observed that though the diesel generator, by operation, works as a grid-forming entity, the nature of $\mathcal{Z}_{\rm P}(s)$ is quite different than that of the GFM IBRs. The fundamental reason is that the leakage reactance of the electrical machine (in this case, a synchronous machine-based diesel generator) along with the droop-based load-frequency control and automatic voltage regulator control change the nature of the the $\mathcal{Z}_{\rm P}(s)$. Although the GFM IBR has the same filter parameters, the phase-locked loop (PLL) control for the GFL IBR causes the different nature of the $\mathcal{Z}_{\rm P}(s)$.

B. Results for Individual DuTs Tested Together

Similarly, using the same theoretical underpinning and the followed approach, the positive-sequence impedance of the DuTs at different perturbation frequencies are individually measured when all DuTs are connected in parallel, as shown in Fig. 6. Note that in this test the harmonic spectrum covers various subharmonic, interharmonic, and higher harmonic components from $f_{\rm h} = 3$ Hz to 477 Hz. The blue circled data

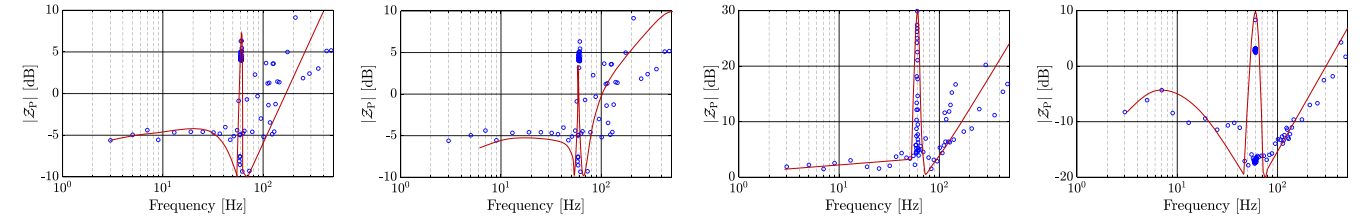

(a) GFM IBR of 125 kVA (b) GFM IBR of 250 kVA (c) GFL IBR of 125 kVA (d) Diesel generator of 187.5 kVA

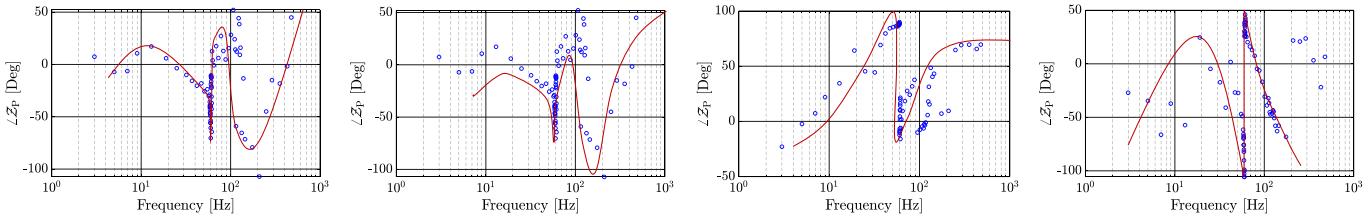

(e) GFM IBR of 125 kVA (f) GFM IBR of 250 kVA (g) GFL IBR of 125 kVA (h) Diesel generator of 187.5 kVA

Fig. 6: The measured positive-sequence impedances of individual DuTs when all are connected in parallel.

TABLE I: Non Piece-wise Transfer Functions of Each DuT with Frequency Range Around Fundamental and Equivalent Damping Coefficients.

DuT	Non-piece-wise Transfer Function	FitPercent
GFM-1	$\frac{0.51357(s+1.116\times10^4)(s+2591)(s-2286)(s-47.47)(s^2+3.287s+1.524\times10^8)}{(s^2+\mathbf{256.3}s+1.432\times10^5)(s^2+883.7s+1.318\times10^8)(s^2+4.365s+1.496\times10^8)}$	96.87%
GFM-2	$\frac{0.51257(s+1.16\times10^4)(s+2155)(s-1995)(s-54.39)(s^2+3.387s+1.523\times10^8)}{(s^2+\mathbf{225.1}s+1.432\times10^5)(s^2+888.9s+1.331\times10^8)(s^2+4.675s+1.493\times10^8)}$	97.62%
GFL	$\frac{3.7061(s+2.371\times10^4)(s+1.41\times10^4)(s+1277)(s+5.944)(s^2+482.7s+7.457\times10^7)}{(s^2+\mathbf{588.1}s+1.423\times10^5)(s^2+506s+5.65\times10^7)(s^2+1551s+1.333\times10^8)}$	97.55%
Gen-Set	$\frac{1.5428(s+1.645\times10^4)(s+8.602)(s^2+1282s+2.088\times10^6)(s^2-2802s+1.012\times10^7)}{(s+8336)(s-4836)(s^2+\mathbf{686.1}s+1.419\times10^5)(s^2+1415s+8.175\times10^6)}$	98.02%

DuT	Damping
GFM-1	$\zeta_{\text{est}}^{\text{dut}} \approx 0.34$
GFM-2	$\zeta_{\text{est}}^{\text{dut}} \approx 0.31$
GFL	$\zeta_{\text{est}}^{\text{dut}} \approx 0.78$
Gen-Set	$\zeta_{\text{est}}^{\text{dut}} \approx 0.91$

are the values computed based on the DuT measurements. The measured magnitude of the positive-sequence impedance, $|\mathcal{Z}_P|$ (in dB), of the GFM IBR of 125 kVA, the GFM IBR of 250 kVA, the GFL IBR of 125 kVA, and the diesel generator of 187.5 kVA, are shown in Fig. 6(a), Fig. 6(b), Fig. 6(c), and Fig. 6(d), respectively. Similarly, the measured phase of the positive-sequence impedance, $\angle\mathcal{Z}_P$ (in deg), of the GFM IBR of 125 kVA, the GFM IBR of 250 kVA, the GFL IBR of 125 kVA, and the diesel generator of 187.5 kVA, are shown in Fig. 6(e), Fig. 6(f), Fig. 6(g), and Fig. 6(h), respectively. An important observation is made here that the nature of the positive-sequence impedance, $\mathcal{Z}_P(s)$, of individual DuTs looks quite similar when the perturbation test is conducted separately to the DuTs (as shown in Fig. 5) and separately while all are connected in parallel (as shown in Fig. 6), especially the nature of $\mathcal{Z}_P(s)$ in a low-frequency spectrum (up to 477 Hz). It demonstrates that the nature of the $\mathcal{Z}_P(s)$ of individual DuTs is agnostic to the other DuTs when connected with the system in parallel. Based on the measured data of the magnitude, $|\mathcal{Z}_P|$, and phase, $\angle\mathcal{Z}_P$, of the positive-sequence impedances of the different DuTs, the best-fit transfer functions (piece-wise) are similarly estimated here, as shown in red. These estimated transfer functions are defined here as $\mathcal{Z}_{P,est}^{gfm1}(s)$ for GFM IBR 1, $\mathcal{Z}_{P,est}^{gfm2}(s)$ for GFM IBR 2, $\mathcal{Z}_{P,est}^{gfl}(s)$ for GFL IBR, and $\mathcal{Z}_{P,est}^{diesel}(s)$ for diesel generator.

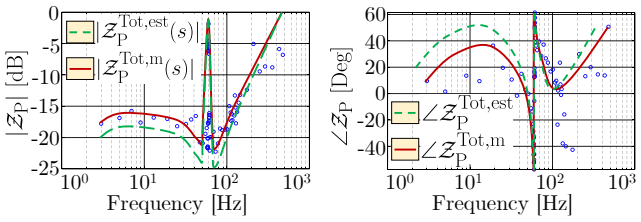

(a) (b)

Fig. 7: The (a) magnitude, $|\mathcal{Z}_P|$ (in dB), and (b) phase, $\angle\mathcal{Z}_P$ (in deg), of the positive-sequence impedance of combined DuTs.

C. Observation and Insights

The measured magnitude and the phase of the positive-sequence impedance, defined as $\mathcal{Z}_P^{Tot,m}(s)$, at different perturbation frequencies for all the DuTs together (i.e., combination of the one GFM IBR of 125 kVA, one GFM IBR of 250 kVA, one GFL IBR of 125 kVA, and one diesel generator of 187.5 kVA) are shown in Fig. 7(a) and Fig. 7(b), respectively. Note that in this test the harmonic spectrum covers various subharmonic, interharmonic, and higher harmonic components from $f_h = 3$ Hz to $f_h = 477$ Hz. In all these figures, the blue circled data are the values computed based on the measurements. Based on the measured data of the magnitude, $|\mathcal{Z}_P^{Tot,m}|$, and phase, $\angle\mathcal{Z}_P^{Tot,m}$, of the positive-sequence impedances of the combined DuTs, the best-fit transfer functions are also estimated here using the same '*tfest*' command of the 'System Identification Toolbox' of MATLAB. In the same figure, the

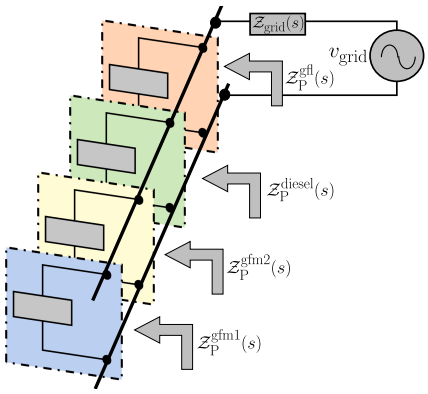

Fig. 8: Parallel connection of multiple DuTs with $\mathcal{Z}_{\rm P}(s)$.

Bode plots of the estimated transfer functions are also shown in red. This estimated transfer function is defined here as $\mathcal{Z}_{\rm P,est}^{\rm Tot}(s)$. Now, according to Fig. 8, the equivalent positive-sequence impedance of the combined DuTs when connected in parallel to each other can be formulated as:

$$\mathcal{Z}_{\rm P}^{\rm Tot,est}(s) = \mathcal{Z}_{\rm P,est}^{\rm gfm1}(s)||\mathcal{Z}_{\rm P,est}^{\rm gfm2}(s)||\mathcal{Z}_{\rm P,est}^{\rm gfl}(s)||\mathcal{Z}_{\rm P,est}^{\rm diesel}(s),$$
$$= \left[\frac{1}{\mathcal{Z}_{\rm P,est}^{\rm gfm1}(s)} + \frac{1}{\mathcal{Z}_{\rm P,est}^{\rm gfm2}(s)} + \frac{1}{\mathcal{Z}_{\rm P,est}^{\rm gfl}(s)} + \frac{1}{\mathcal{Z}_{\rm P,est}^{\rm diesel}(s)}\right]^{-1}.$$

The Bode magnitude and phase plot of the computed $\mathcal{Z}_{\rm P}^{\rm Tot,est}(s)$ are also shown in Fig. 7(a) and Fig. 7(b) in green. The small mismatch between $\mathcal{Z}_{\rm P}^{\rm Tot,m}(s)$ and $\mathcal{Z}_{\rm P}^{\rm Tot,est}(s)$ is mainly due to the accumulated errors in the estimation method in the curve fitting, as tabulated in Table I. It is observed that the nature of $\mathcal{Z}_{\rm P}^{\rm Tot,est}$ of the combined DuTs is quite similar to that of the equivalent positive-sequence impedances, $\mathcal{Z}_{\rm P}^{\rm Tot,m}$. It demonstrates that the positive-sequence impedance of the DuT is agnostic to the other DuTs connected in parallel.

As shown in Fig. 5, Fig. 6 and Fig. 7, the positive-sequence impedances exhibit a resonating peak behavior at the fundamental frequency ($\omega_{\rm R} = 2\pi 60$). The wide nature of the peak determines the equivalent damping of the resonance. The closest non-piece-wise transfer functions of $\mathcal{Z}_{\rm P,est}^{\rm gfm1}(s)$, $\mathcal{Z}_{\rm P,est}^{\rm gfm2}(s)$, $\mathcal{Z}_{\rm P,est}^{\rm gfl}(s)$ and $\mathcal{Z}_{\rm P,est}^{\rm diesel}(s)$ are tabulated in Table I. For quantitative assessment of the estimation, the 'tfest' provides a variable called, $\rm FitPercent{:=}100 \times (1 - NRMSE)\%$ where NRMSE is the normalized root mean squared error, that measure how well the response of the model fits the estimation data, tabulated in Table I. It is important to mention here that these transfer functions are non-piece-wise estimated transfer functions which represent the piece-wise transfer functions of Fig. 6 only inside the frequency-range around the fundamental frequency, used in piece-wise transfer function computation. Now, based on the estimated and best-fit transfer function for each measured positive-sequence impedance, the equivalent damping coefficient, $\zeta_{\rm est}^{\rm dut}$, for each individual DuT as well as the combined DuTs can be computed. It is observed that the equivalent damping coefficient, $\zeta_{\rm est}^{\rm dut}$, for both commercial GFM IBRs of 125-kVA and 250-kVA rating are ≈ 0.34 ($2\zeta_{\rm est}^{\rm dut}\omega_{\rm R} \approx 256.3$) and ≈ 0.31 ($2\zeta_{\rm est}^{\rm dut}\omega_{\rm R} \approx 225.1$), respectively, These are less than the other two DuTs, i.e., the GFL IBR and the diesel generator. $\zeta_{\rm est}^{\rm dut}$ for GFL IBR and the diesel generator are ≈ 0.78 ($2\zeta_{\rm est}^{\rm dut}\omega_{\rm R} \approx 588.1$) and ≈ 0.91 ($2\zeta_{\rm est}^{\rm dut}\omega_{\rm R} \approx 686.1$), respectively. Note that of the four types of DuTs, the diesel generator exhibits the highest equivalent damping in the positive-sequence impedance. This also indicates the enhanced stability in the operation of the diesel generator compared with the GFM and GFL IBR.

IV. Conclusion

Two GFM IBRs, a GFL IBR, and a diesel generator are considered as DuTs for the impedance scan using pure hardware setup. By injecting perturbed voltage signals and by measuring the current response, the positive-sequence impedances are computed and the best-fit transfer functions are estimated that closely resemble the measured data points. The key findings of this study are: 1) the positive-sequence impedance of GFM-IBR is agnostic to the power ratings and capacitive in nature at fundamental frequency; whereas for GFL-IBR, it's magnitude is higher and less capacitive in comparison with GFM-IBRs; for diesel generator the magnitude is higher compared with GFM-IBRs, 2) the positive-sequence impedances measured individually, when DuTs are connected in parallel and isolated to each other, are similar in nature, and 3) diesel generator and GFL-IBR provide more damping in the system than GFM-IBRs. As future work, these measured impedances will be utilized for impedance/admittance-based stability assessment of power grids interfaced with IBRs and generators.

References

[1] Y. Gu and C. T. Green, "Power system stability with a high penetration of inverter-based resources," in *Proceedings of the IEEE*, vol. 111, no. 7, 2023, pp. 832–853.

[2] L. Fan *et al.*, "Real-world subsynchronous oscillation events in power grids with high penetrations of inverter-based resources," *IEEE Transactions on Power System*, vol. 14, no. 1, pp. 734–738, 2023.

[3] L. Ding *et al.*, "Small-signal stability support from dynamically configurable grid-forming/following inverters for distribution systems," in *2022 IEEE Energy Conversion Congress and Exposition (ECCE)*. IEEE, 2022, pp. 1–5.

[4] H. Hosseinpour, M. MansourLakouraj, M. Ben-Idris, and H. Livani, "Lyapunov-based large-signal stability analysis of inverter-based microgrids," in *2022 North American Power Symposium (NAPS)*. IEEE, 2022, pp. 1–5.

[5] H.-D. Chiang, M. W. Hirsch, and F. F. Wu, "Stability regions of nonlinear autonomous dynamical systems," *IEEE Transactions on Power System*, vol. 33, no. 1, pp. 16–27, 1988.

[6] S. Shah, P. Koralewicz, V. Gevorgian, H. Liu, and J. Fu, "Impedance methods for analysizing the stability impacts of inverter-based resources," in *2021 IEEE Electrification Magzine*. IEEE, 2021, pp. 53–65.

[7] "Great britain grid forming best practice guide," 2024.

[8] L. Harnefors, X. Wang, A. G. Yepes, and F. Blaabjerg, "Passivity-based stability assessment of grid-connected vscs—an overview," *IEEE Journal of emerging and selected topics in Power Electronics*, vol. 4, no. 1, pp. 116–125, 2015.

[9] M. Cespedes and J. Sun, "Impedance modeling and analysis of grid-connected voltage-source converters," *IEEE Transactions on Power Electronics*, vol. 29, no. 3, pp. 1254–1261, 2013.

[10] S. Shah and L. Parsa, "Impedance modeling of three-phase voltage source converters in dq, sequence, and phasor domains," *IEEE Transactions on Energy Conversion*, vol. 32, no. 3, pp. 1139–1150, 2017.

[11] S. Shah, P. Koralewicz, R. Wallen, and V. Gevorgian, "Impedance characterization of utility-scale renewable energy and storage systems," in *2019 IEEE Energy Conversion Congress and Exposition (ECCE)*. IEEE, 2019, pp. 2609–2616.

[12] W. Yan, S. Shah, V. Gevorgian, and D. W. Gao, "Sequence impedance modeling of grid-forming inverters," in *2021 IEEE Power & Energy Society General Meeting (PESGM)*. IEEE, 2021, pp. 1–5.